Quantum size effect driven thermal decomposition of Ag films on Fe(100) in the presence of pinhole-growth morphological defects

K. L. Man,[1] Z. Q. Qiu,[1,2] and M. S. Altman[1,*]
[1]*Department of Physics, Hong Kong University of Science and Technology, Clear Water Bay, Kowloon, Hong Kong*
[2]*Department of Physics, University of California at Berkeley, Berkeley, California 94720, USA*
(Received 25 June 2009; revised manuscript received 31 October 2009; published 26 January 2010)

The growth morphology of Ag films that are deposited on an Fe(100) surface at room temperature has been investigated using low-energy electron-diffraction spot-profile analysis and low-energy electron microscopy. The superposition of periodic spot-profile modulations that are caused by interference of waves that are reflected from the surface at different exposed levels and intensity oscillations that are associated with quantum-well resonances within the film provides complementary information on film roughness and thickness. The predominant morphological defect that is present during layer-by-layer growth is determined to be pinholes that penetrate completely through the film to the Fe substrate surface. Such imperfect films are observed to decompose upon annealing to thicknesses that are stabilized by quantum-well states. This result suggests that pinholes eliminate kinetic limitations that promote the unusual bifurcation mode of thermal decomposition that was observed previously for atomically smooth films prepared at low temperature.

DOI: 10.1103/PhysRevB.81.045426 PACS number(s): 68.55.−a, 68.65.Fg, 61.05.jh, 68.37.Nq

I. INTRODUCTION

Quantum-size effects (QSEs) in the properties of thin metal films and islands may occur due to the influence of discrete quantum-well (QW) states that are caused by electron confinement.[1–3] Properties will be influenced to varying degrees depending upon the proximity of QW state binding energies to the Fermi energy. The binding energies of QW states are determined by several factors, including bulk band dispersion and film thickness. It is often found that QW states periodically cross the Fermi level with increasing film or island thickness. The resultant modulation of the density of states at the Fermi level has been linked to the periodic variation in many physical and chemical properties. QW states can also induce a similar modulation of the confined electron energy. This has the potential to define a sequence of stable and unstable island heights or film thicknesses with the same periodicity that QW states pass through the Fermi level. As a consequence, film morphology can be dominated during growth or annealing by film thicknesses that support the most strongly bound QW states. Evidence of a QSE in film and island morphology has been observed for many metals on various substrates.[3–14] This effect is envisioned to be a mechanism for exercising control over island or film morphology. Such a capability to control the dimensions of nanostructures is essential for varying and controlling their electronic structure and properties. However, kinetic-growth limitations may interfere with the control over morphology that is promised by QSE driven energetics.[6,7,10] Therefore, attention has recently turned toward the kinetics of the self-organization of QSE-induced island and film morphology.[12,13,15]

Ag films on the Fe(100) surface have received attention because of the impact of QW states on film energetics, morphology, and thermal stability.[6,10,16] The small lattice mismatch (0.7%) between a Ag film and the Fe(100) substrate results in a system that is almost strain free. This means that stress-induced effects in film morphology[17] should not come into play and we may therefore concentrate on electronic effects. The stability of 2- and 5-monolayer(ML)-thick Ag films during annealing and growth at high temperature is associated with strongly bound QW states at the $\bar{\Gamma}$ point, which induce total-energy local minima compared to intermediate thicknesses. The instability of the intermediate thicknesses is interesting because their thermal-decomposition products depend upon the film-preparation method.[6,10] With the exception of stable 2- and 5-ML-thick films, atomically flat N ML films (N=integer) prepared by low-temperature deposition methods were reported to transform, or bifurcate, to a combination of $N-1$ and $N+1$ thick regions during annealing above room temperature.[6] The origin of this unusual behavior can be traced to the shape of the local energy versus thickness landscape defined by QW states in $N-1$, N, and $N+1$ thick films. The negative curvature of the energy landscape between QW-induced energy local minima results in a reduction in the system energy for the bifurcation mode of decomposition.[6,16] Investigations of Ag films that were grown at room temperature confirmed the stability of 2 and 5 ML films and instability of 3 and 4 ML films during annealing.[10] However, 3 and 4 ML films were observed to decompose to stable 2 and 5 ML components, instead of their respective bifurcation morphologies. The suppression of the bifurcation mode of decomposition was tentatively attributed to film roughness or some other morphological defect that is introduced during growth at room temperature,[10] although no direct evidence of this film imperfection was provided. Such film imperfection apparently reduces or eliminates the kinetic barrier that traps initially flat, unstable films in their respective metastable bifurcation morphologies during decomposition.

In the present work, we take a closer look at the growth morphology of Ag films that are prepared by deposition at room temperature. We also characterize the morphological evolution that occurs during their thermal decomposition in greater detail than reported earlier. One of the aims of this investigation is to understand the nature of the growth mor-

phological defect that impacts on the thermal-decomposition mode. Our approach to studying film growth morphology is to examine the interference of electron waves that are reflected from different exposed levels at the surface. This interference produces oscillations of the low-energy electron-diffraction (LEED) spot profile vs energy.[5,18–20] Measurements are carried out in the very low energy range where the electron mean-free path is long. The resulting deep penetration of electrons through the film facilitates the additional interference of the electron waves that reflect from the film surface and from the buried interface.[10] This phenomenon is analogous to the interference that gives rise to intensity oscillations as a function of perpendicular momentum transfer in x-ray reflectivity measurements of thin films.[21,22] In the case of electrons, constructive interference peaks that are observed in oscillations of the reflected intensity are associated with QW resonances above the vacuum level.[10,23] The superposition of these two interference phenomena simultaneously provides complementary information on nominal film thickness and roughness, which characterize film morphology more completely.

We find that pinholes that penetrate through the entire thickness of the film to the substrate surface are the predominant morphological imperfection that is introduced during growth at room temperature. The presence of pinholes may very likely be the reason why the bifurcation mode of thermal decomposition is not prevalent for these films. In particular, we find that 3 ML films decompose directly into 2 and 5 ML thicknesses that are stabilized by quantum-well states, whereas this decomposition mode prevails for 4 ML films only after their partial decomposition by bifurcation.

II. EXPERIMENTAL RESULTS

A. Experimental details

The Fe(100) single-crystal substrate was cleaned by extensive Ar^+ ion sputtering and annealing cycles. Ag was deposited from an electron-beam-heated source at a typical rate of 0.3 ML/min. LEED measurements of the (00) beam at normal incidence, corresponding to no momentum transfer parallel to the surface, were performed in a low-energy electron microscope (LEEM).[24,25] These new LEED data are presented here in comparison to results of LEEM-image intensity measurements that were obtained previously for the same diffraction condition [Fig. 1(a)].[10] The LEED instrumental transfer width, which is essentially the lateral coherence length of the probe electrons, is on the order of 25 nm.[26] The angular acceptance of a contrast aperture that is used in the LEEM imaging mode corresponds to a parallel momentum transfer of 0.12 $Å^{-1}$. This equates with a lateral correlation length of 5 nm. Unlike conventional LEED instruments, the LEED transfer width and LEEM angular acceptance do not change with energy because of the compensating action of the objective lens on electron trajectories.[25]

B. Growth morphology

In the previous study,[10] LEEM was used to detect peaks in the elastically reflected electron intensity at very low energy

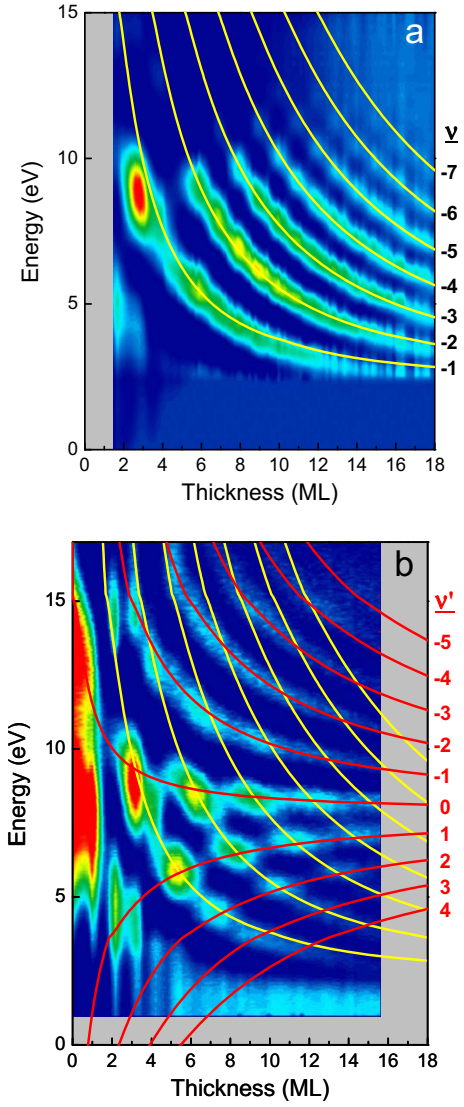

FIG. 1. (Color) The (a) integrated LEEM intensity (from Ref. 10) and (b) p-ratio of the (00) LEED spot profile vs incident electron energy and thickness (ML=monolayer) for Ag films grown on Fe(100) at 300K. The solid yellow and red lines through the data are the phase accumulation [Eq. (1)] and two-level interference [Eq. (5)] model predictions, respectively, for the values of the quantum numbers, ν and ν', that are indicated on the right.

that are associated with QW resonances above the vacuum level [Fig. 1(a)]. The dependence of the reflected intensity upon film thickness and incident electron energy was determined by measuring the LEEM-image intensity continuously during deposition at room temperature while repeatedly ramping the incident energy from 0 to 15 eV. The LEEM-image measurement effectively integrates diffracted intensity in the vicinity of the (00) diffraction position over an area of the Brillouin zone that is large enough to encompass all or nearly all of the diffraction spot profile. After normalizing the LEEM-image-intensity data by the intensity spectrum of a thick Ag film (Fig. 2), intensity peaks are clearly seen that increase in number and disperse toward lower energy with increasing film thickness [Fig. 1(a)]. This normalization suppresses the signal from a strong Bragg peak that is caused by

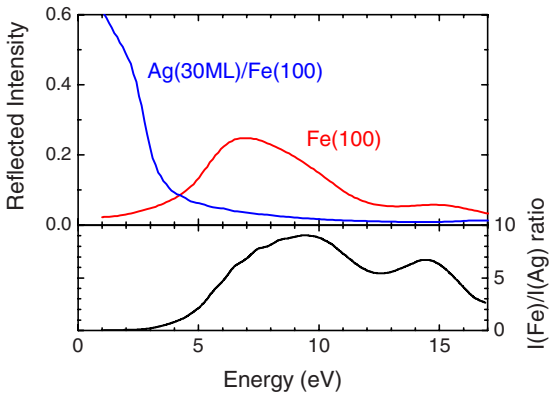

FIG. 2. (Color online) Absolute reflected intensity vs energy, $I(V)$, curves of the specular (00) diffraction at normal incidence obtained from LEEM imaging for a bulk Fe(100) crystal surface and 30 ML Ag film on Fe(100). The ratio of Fe- and Ag-reflected intensities is shown in the bottom of the figure.

a band gap at vacuum level[27] so that the intensity peaks associated with QW resonances can be discerned more clearly.

Essentially, intensity peaks associated with QW resonances are produced by constructive interference between the wave that is reflected from the film surface and the wave that travels through the film and reflects from the buried interface. The QW resonance conditions that are identified by the peaks in the LEEM-intensity spectra were described accordingly by the phase-accumulation model.[10] According to this model,[28] the quantization condition for the existence of QW states and resonances is $2k(E)mt+\Phi_C(E)+\Phi_B(E)=2n\pi$, where $k(E)$ is the perpendicular wave vector of an electron in the film, m is the number of atomic layers, t is the layer spacing, $\Phi_C(E)$ and $\Phi_B(E)$ are the energy-dependent phase shifts that occur upon reflection at the interface and surface,[29] respectively, and n is an integer. The quantization condition can be inverted[28] to find an expression for the thickness at which a QW state or resonance exists at a given energy

$$m = \frac{[\Phi_C(E) + \Phi_B(E)]/2\pi + \nu}{\kappa(E)/k_{BZ}}, \tag{1}$$

where the quantum number $\nu=m-n$, $k_{BZ}=\pi/t$, and the wave vector $\kappa(E)=k_{BZ}-k(E)$ is measured from the Brillouin-zone boundary in the direction perpendicular to the film plane, i.e., the X point for Ag(100).

The resonance conditions that were calculated for Ag/Fe(100) using Eq. (1) were found in Ref. 10 to match the experimental resonance peaks in Fig. 1(a) very well with no adjustable parameters. For this calculation, the $\kappa(E)$ in Eq. (1) are given by an sp band with Δ_1 symmetry that lies just above the vacuum level in Ag(100).[10,30,31] The interface reflection phase is evaluated using an empirical formula,[23,28,31] $\Phi_C(E)=2\arcsin\sqrt{(E-E_L)/(E_U-E_L)}-\pi$, where $E_L=5.0$ eV and $E_U=15.5$ eV (above the vacuum level) are the lower and upper edge of the Fe band gap, respectively.[32] It was also found empirically in Ref. 10 that the phase shift at the surface is negligible, $\Phi_B(E)=0$. This can be expected from the fact that the reflection and transmission amplitudes are both real and positive at energies above a potential step, such as the surface-barrier potential.

The results in Fig. 1(a) indicate that layer-by-layer growth at 300 K results in a nominally flat film or at least that the film is flat enough on the length scale of the LEEM lateral resolution, ~10 nm, that the intensity peaks produced by QW resonances are not smeared out. Here, we obtain complementary information on film morphology on a lateral length scale shorter than the LEED instrumental transfer width, ~25 nm,[26] by examining the LEED spot profile. The measured intensity in a surface-diffraction experiment can be written[5,18–20] as a sum of a narrow, instrumentally limited component, $\delta(k_\parallel)$, and a broad component, $L(k_\parallel)$

$$I(k_\parallel,k_\perp) = A(k_\perp)\delta(k_\parallel) + B(k_\perp)L(k_\parallel), \tag{2}$$

where $k_\perp$ and $k_\parallel$ are the momentum transfer perpendicular and parallel to the surface, respectively. Only the narrow component is present for a flat surface under all scattering conditions. The presence of multiple exposed levels, or terraces, separated by atomic steps at a surface redistributes intensity away from the narrow component for a flat surface and into the broad component. The redistribution of intensity is greatest in out-of-phase scattering conditions between adjacent levels. This occurs when the scattering phase $\phi=k_\perp t$ is an odd multiple of π, where the step height, t, is taken to be equal to the layer spacing. On the other hand, the broad component is suppressed and the diffraction measurement is insensitive to the presence of different levels when the scattering phase is an even multiple of π at in-phase scattering conditions. The dependence of the complementary functions, $A(k_\perp)$ and $B(k_\perp)$, upon $k_\perp$ reflects the vertical arrangements of levels while the dependence of the broad component lineshape, $L(k_\parallel)$, upon $k_\parallel$ is determined by the lateral arrangements.

Although the lineshape and width of the broad component, $L(k_\parallel)$, are affected by the terrace-size distribution and average terrace size, respectively, its integral over $k_\parallel$ in the surface Brillouin zone is not. The integral of the narrow component lineshape, $\delta(k_\parallel)$, is similarly independent of the island distribution. These integrals are only affected by the atomic scattering factor and structure factor. This dependence can be factored out by evaluating the normalized intensity in the narrow component which is constructed out of the integrals over the surface Brillouin zone

$$p = \frac{A(k_\perp)\int\delta(k_\parallel)d^2k_\parallel}{A(k_\perp)\int\delta(k_\parallel)d^2k_\parallel + B(k_\perp)\int L(k_\parallel)d^2k_\parallel}. \tag{3}$$

For measurements of the specular (00) beam, it has been shown that the proportion of intensity in the narrow component given by the p-ratio in Eq. (3) is a one-dimensional sum over the exposed levels according to the following form:[19]

$$p(k_\perp) = \left|\sum_{n=1}^{N}\theta_n \exp(ik_\perp nt)\right|^2, \tag{4}$$

where θ_n is the area fraction exposed to vacuum at level n and $N-1$ is the distance between the top and bottom exposed levels in units of the elemental step height. The oscillatory

dependence of the p-ratio on $k_\perp$ can provide information on the step height and the areas of the exposed levels.

The dependence of the p-ratio, Eq. (3), upon film thickness and incident electron energy for Ag/Fe(100) is determined from measurements of the diffraction spot profile that were made continuously during deposition at room temperature while the incident energy was repeatedly ramped from 1 to 17 eV. The dynamic range of the LEED-intensity profile measurement in the LEEM is not sufficient to extract the weak, broad profile component reliably at all energies and for all film thicknesses. To address this problem, we note that the LEEM-image intensity effectively integrates both broad and narrow components, as pointed out above. The integrated LEEM-image intensity for a thick Ag film ($\sim$30 ML) on Fe(100) (Fig. 2) therefore serves as a good approximation of the sum of integrals in the denominator of Eq. (3), excluding the effect on intensity of QW resonances. The result for the p-ratio using this approximate normalization is shown in Fig. 1(b). Because of the approximate normalization used to calculate the p-ratio neglects the effect of QW resonances, the peaks that are seen in the lower energy range in Fig. 1(b) are defined in part by QW resonances in the Ag film. This is demonstrated by overlaying the dispersion of QW resonance conditions in Fig. 1(b) that were modeled by the phase accumulation model [Eq. (1)] and are displayed already in Fig. 1(a). Besides the impact of QW resonances, an additional modulation is also seen in Fig. 1(b) that is due to interference of waves that are reflected from the surface at different exposed levels. This should be describable by the form of the p-ratio given by Eq. (4).

Although roughness of the Ag film surface potentially exposes many levels, the data indicate that the roughness-induced modulation in Fig. 1(b) is dominated by interference between only two levels. In particular, the data can only be accounted for by a two-level interference between the film and substrate surfaces (see the following paragraph and Sec. III A for further discussion of this point). For such a two-level system, the p-ratio for the specular (0,0) beam given by Eq. (4) simplifies to, $p=\tilde{\theta}_0^2+\theta_m^2+2\tilde{\theta}_0\theta_m\cos\phi$, where the indices 0 and m refer to the substrate surface and the film surface, respectively, m is the number of atomic layers in the film, and ϕ is the total phase shift between waves that are reflected from the two levels. The term $\tilde{\theta}_0$ is the effective area fraction of the substrate, the meaning of which will be discussed below. For now, we are mainly interested in the phase.

LEED spot-profile analysis of surface roughness is normally applied in the case that the exposed levels are of the same material. In that case, any additional scattering phase that is introduced by reflection at different levels should be the same. Consequently, the scattering phase cancels in the calculation of the total phase shift and the phase shift between adjacent levels is caused only by the path-length difference. However, since the two levels that are being considered here are of different material, Fe substrate and Ag film surfaces, we must include the additional respective scattering phases that are introduced on reflection from the film surface, $\Phi_B'(E)$, and substrate surface, $\Phi_C(E)$, explicitly in the calculation of the total phase shift. This leads to an expression for the constructive interference condition between levels that resembles the phase-accumulation model, $k'(E)mt+\Phi_C(E)-\Phi_B'(E)=2n'\pi$, where $k'(E)=k_\perp=2(2\pi/\lambda)$ is the perpendicular momentum transfer in vacuum, $\lambda\approx\sqrt{150/E}$ is the wavelength in Angstrom, E is the incident energy, n' is an integer, and the remaining terms are defined as above.[33] This can be inverted to find an expression for the thickness at which constructive interference between levels occurs at a given energy

$$m=\frac{[\Phi_C(E)-\Phi_B'(E)]+2\pi\nu'}{\kappa'(E)t}, \tag{5}$$

where the quantum number $\nu'=m-n'$, the modified momentum transfer is $\kappa'(E)=2\pi/t-k'(E)$, and $2\pi/t$ is the fundamental momentum transfer for constructive interference at a single step, $k_\perp=2\pi n'/mt$ for $m=1$ and $n'=1$, neglecting $\Phi_C(E)$ and $\Phi_B'(E)$. Setting $\Phi_B'(E)=0$ for the reason given above and using the empirical expression given above for $\Phi_C(E)$,[23,28] Eq. (5) produces the set of curves for different values of ν' that are shown in Fig. 1(b). These curves pass through the maxima in the figure with no fit parameters. This confirms the conjecture that a two-level interference between substrate and film surfaces is responsible for the modulation of the LEED spot profile. No other two-level or multiple-level interference model can explain the data.

Interestingly, the ν' curves in Fig. 1(b) exhibit a change in curvature between $\nu'>0$ and $\nu'\leq 0$. This is reminiscent of metallic QW state dispersion above and below a band edge, e.g., compare the dispersion of QW states[28] and resonances [Ref. 10 and Fig. 1(a)] for Ag/Fe(100). To understand the shapes of these curves, recall the inverse relation between real-space dimension of an object and the separation of reciprocal space features that it produces. A single-atomic step produces constructive interference conditions at the kinematic Bragg conditions and destructive interference at the anti-Bragg condition, i.e., midway (in perpendicular momentum transfer) between Bragg conditions. A double height atomic step on the other hand produces an additional constructive interference condition at the anti-Bragg condition. The $\nu'=0$ curve is basically related to the constructive interference condition between levels that are separated by a double height step. In the limit of large thickness, the $\nu'=0$ curve converges with the constructive interference condition for a double step between Ag levels on the Ag film. The $\nu'=0$ curve bends upward as thickness is decreased because of the contribution of the additional phase Φ_C that is generated by scattering from the Fe substrate at the bottom of pinholes. Specifically, the phase shift produced by the path-length difference between the top and bottom of pinholes decreases with decreasing film thickness. But, Φ_C is independent of thickness. That means that the double-step constructive interference condition is perturbed more by the Φ_C contribution as thickness is decreased. That gives rise to the deviation of the $\nu'=0$ curve from the constructive condition for a double Ag step. The $\nu'>0$ and $\nu'<0$ curves have opposite curvature. The reason is that increasing pinhole height forces more constructive interference conditions between Bragg conditions. For an m-layer height object, there will be $m-1$ con-

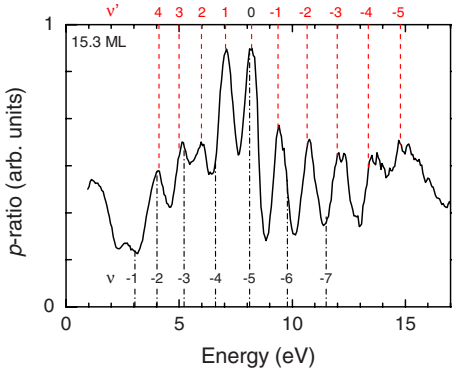

FIG. 3. (Color online) The dependence of the p-ratio (Eq. (3)) on incident electron energy is shown for a Ag film thickness of 15.3 ML. The positions of peaks due to interference between exposed levels that are predicted for pinholes that penetrate to the Fe substrate are indicated by dashed lines and ν' indices. The positions of peaks due to QW resonances are indicated by dot-dashed lines and ν indices.

structive interference conditions between Bragg conditions. Again, that is the usual inverse relationship between real and reciprocal space.

The area fraction of each level can also be determined, in principle, by evaluating the Fourier transform of the p-ratio modulation. A good estimate of the area fractions can be made quickly by comparing the modulation amplitude, $2\tilde{\theta}_0\theta_m$, to the maxima, $\tilde{\theta}_0^2+\theta_m^2+2\tilde{\theta}_0\theta_m$, that are prescribed by the simple form for a two-level system that is given above. Figure 3 shows the p-ratio vs energy at Ag film coverage of 15.3 ML, where QW resonance peaks are weak, particularly above 9 eV. The modulation of the p-ratio in the range 9–14 eV suggests that the effective area fraction of the substrate surface is approximately $\tilde{\theta}_0 \approx 0.15-0.20$. However, it is important to note that this value represents the actual area fraction weighted by the relative reflectivity of the substrate and the film. Since the reflectivity of the Fe substrate is greater by an average factor of about $7\times$ in the relevant energy range (Fig. 2), the actual exposed substrate area fraction, θ_0, is roughly estimated to be smaller than the effective area fraction, $\tilde{\theta}_0$, by this amount, i.e., on the order of $\theta_0 \sim 0.025$. Considering that QW resonance peaks may also contribute to the modulation of the p-ratio, this should be treated as an upper limit of the area exposed by pinholes.

C. Thermal decomposition

The thermal decomposition of Ag films was characterized by monitoring LEEM images and by recording area-integrated intensity vs voltage $[I(V)]$ spectra in imaging mode during annealing. The $I(V)$ spectra obtained in imaging mode represent the (00) specular beam intensity at normal incidence, corresponding to no parallel momentum transfer. They are analogous to the normalized $I(V)$ data presented pictorially in Fig. 1(a). The aim of integrating the intensity over a large area in the image was to detect any spectroscopic signature of thermal decomposition while the lateral dimension of the decomposition products is small, i.e., below

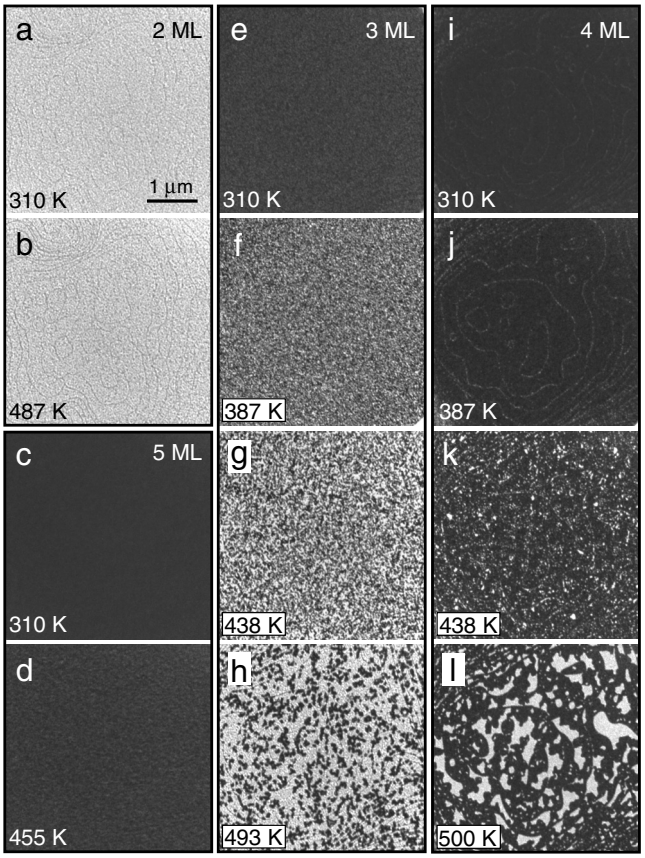

FIG. 4. LEEM images of initially [(a) and (b)] 2 ML, [(c) and (d)] 5 ML, [(e)–(h)] 3 ML, and [(i)–(l)] 4 ML Ag films at the temperatures indicated during annealing. The imaging energy was 4.5 eV. Panels (h) and (l) are from Ref. 10.

the imaging resolution and therefore undetected by imaging. The positions of peaks that are present in the spectra can be used to identify what the decomposition products are.

LEEM images and $I(V)$ spectra were recorded at several temperatures while heating the film incrementally up to about 500 K. Images obtained sequentially at successively higher temperatures are shown in Fig. 4 for different initial film thicknesses. The evolution of the corresponding $I(V)$ spectra that were obtained during the same annealing sequences are shown in Fig. 5. Insignificant changes in the appearance of initially 2 and 5 ML films in images [Figs. 4(a)–4(d)] and of the peak positions in the respective $I(V)$ spectra (Fig. 5) are observed during annealing. These results confirm the stability of 2 and 5 ML films. This behavior contrasts with dramatic changes in the images [Figs. 4(e)–4(l)] and spectra (Fig. 5) of initially 3 and 4 ML films that occur during annealing. The morphological changes in the 3 ML film are initiated at numerous small nuclei that are randomly distributed over the surface [cf. Fig. 4(f)]. These nuclei grow and coarsen as the temperature is raised. Although morphological changes in the 4 ML film appear to start at step edges [cf. Fig. 4(j)], randomly located nuclei again proliferate and coarsen as the temperature is raised. The $I(V)$ spectra measured locally in the distinct regions that are produced by thermal decomposition of 3 and 4 ML films were found to resemble the spectra of the stable 2 and 5 ML

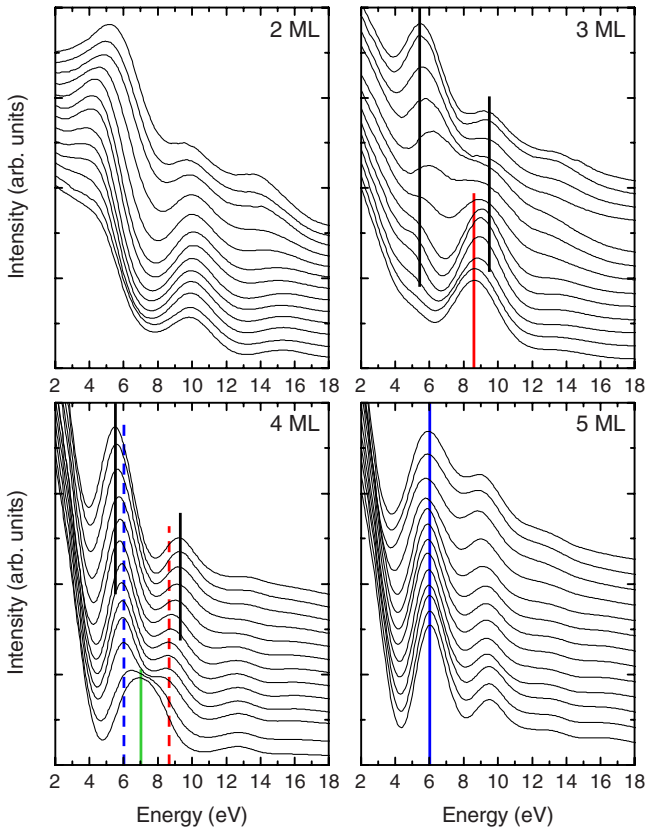

FIG. 5. (Color online): $I(V)$ spectra for initially 2–5 ML Ag films are shown at various temperatures during annealing. Spectra from bottom to top that were obtained at 310, 320, 337, 354, 363, 372, 387, 400, 420, 438, 455, 474, and 490 K are shifted vertically for clarity. Prominent peaks in the initial spectra of the 3, 4, and 5 ML films are identified by solid red, green, and blue lines at 8.7, 7.0, and 6.0 eV, respectively. The dashed red and blue lines in the 4 ML spectra plot locate the initial 3 ML (8.7 eV) and 5 ML (6.0 eV) peak positions. The solid black lines in the 3 and 4 ML spectra locate the final peak positions after thermal decomposition.

films.[10] The area fractions of the 2 and 5 ML regions following decomposition were also found to be consistent with the mass of the initial films.[10] These observations demonstrate that 3 and 4 ML films decompose to thicknesses stabilized by QWs.

Closer examination of the spectra at different stages during annealing reveals interesting details of the thermal-decomposition pathway. Spectra for 3 and 4 ML films initially exhibit prominent peaks at 8.7 and 7.0 eV, respectively, at room temperature. For the 3 ML film, this dominant peak begins to shift toward higher energy at about 340 K. A small peak also begins to grow slowly at about 5.2 eV at the same temperature. The final positions of these two peaks after thermal decomposition is complete are 9.4 and 5.5 eV, respectively. The peak at 9.4 eV can be attributed to the presence of the mixture of 2 and 5 ML film components after decomposition, which individually produce peaks at 10 and 9.1 eV, respectively. Likewise, the peak at 5.5 eV is produced by the combination of 2 and 5 ML peaks at 5.2 and 6.0 eV, respectively. Above all, no evidence is seen in the 3 ML spectra during thermal decomposition of a peak at 7.0 eV that would be indicative of a 4 ML film component. From the absence of this 4 ML signature, we conclude that the 3 ML film decomposes directly to 2 and 5 ML regions without any prevalence for bifurcation.

For the 4 ML film, the dominant peak at 7.0 eV begins to broaden already at 320 K. At 337 K, this broadening is clearly resolved as a splitting into two distinct peaks, at 8.7 and 6.0 eV. These peaks remain stationary until 387 K when they begin to shift up to 9.2 eV and down to 5.5 eV, respectively. The intermediate peaks at 8.7 and 6.0 eV are signatures of 3- and 5-ML-thick regions, respectively. Similar to the case of the initial 3 ML film, the final peak positions at 9.2 and 5.5 eV are both associated with the presence of a mixture of 2 and 5 ML film products following thermal decomposition. Thus, we find evidence of bifurcation between 320 and 387 K and that this mode is overcome at higher temperature by decomposition to 2 and 5 ML thicknesses. However, it is not possible to determine the proportion of the film that bifurcates below 387 K based upon these data.

III. DISCUSSION

A. Growth morphology

The growth morphology of Ag films that are deposited on an Fe(100) surface at room temperature has been investigated in order to understand better the origin of their QSE driven thermal-decomposition behavior. Film thickness is determined from oscillations of the elastically reflected electron intensity vs incident electron energy that are associated with QW resonances. These oscillations are derived from the interference of the wave that is reflected from the film surface and the wave that travels through the film and reflects from the buried interface. Information about surface roughness is also obtained by examining modulations of the LEED spot profile that are caused by interference of waves that are reflected from different exposed levels at the film surface. The complementary information that is obtained by evaluating these two interference phenomena reveals that the predominant morphological defect is pinholes that penetrate completely through the film to the exposed Fe substrate surface.

In order to shed light on the validity of these results, we briefly reiterate the principles of the methods that were used. The deep electron penetration of electrons at very low energy facilitates the interference between waves that are reflected from the film surface and the buried interface. The intensity oscillations that are shown in Fig. 1(a) are indeed produced by such interference. Intensity peaks in Fig. 1(a) identify constructive interference conditions that are associated with QW resonances in the case of electrons. The QW resonances provide information on film thickness. This is analogous to the interference that gives rise to intensity oscillations as a function of perpendicular momentum transfer in x-ray reflectivity measurements of thin films.[21,22] In the case of x-rays, intensity oscillations contain information about film thickness and roughness. The oscillation period is related to the inverse of the thickness. The oscillation amplitude is proportional to the density difference between film and substrate. Surface and interface roughness are manifested in the decay of the scattered x-ray intensity and damping of the intensity

oscillations with increasing momentum transfer.

On the contrary, information on the surface morphology is ascertained here by examining a quantity called the *p*-ratio, Figs. 1(b) and 3, which is obtained from diffraction spot-profile analysis. The *p*-ratio is not equivalent to the intensity that is recorded in x-ray reflectivity measurements. Instead, it is the normalized intensity in the narrow component of the diffraction spot profile. The dependence of the narrow component intensity on the perpendicular momentum transfer reflects the vertical arrangements of exposed levels, i.e., the surface morphology.[5,18–20] It is defined in Eq. (3) as the integrated (over the Brillouin zone) intensity within the narrow profile component divided by the sum of the integrals of the narrow and broad components, i.e., the total integrated intensity. Thus, the *p*-ratio is a normalized "partial" integrated intensity. This definition of the *p*-ratio factors out the dependence of the integrated intensity in the narrow component on the atomic-scattering factor and structure factor. In our work, the sum of the narrow and broad component integrals in the denominator of the *p*-ratio is approximated by the integrated LEEM intensity for a thick Ag film. This does not account for the x-raylike interference between the waves that are reflected from the surface and buried interface, which give rise to the intensity oscillations in Fig. 1(a). As these features are not accounted for by the approximate normalization that we use, they show up as artifacts in the plot of the *p*-ratio in Fig. 1(b). The constructive interference or QW resonance conditions are delineated by yellow lines in these two figures. Besides the x-raylike intensity oscillations that are associated with QW resonances, an additional modulation is observed in the *p*-ratio in Fig. 1(b) that is caused by the interference between waves that are reflected from exposed levels at the surface. The features that are attributable to the surface morphology are connected by red lines with indices ν' in Fig. 1(b).

Are there any pinholes? The conclusion about the presence of pinholes is based on the positions of a subset of oscillation features in the *p*-ratio in Fig. 1(b), not the oscillation amplitudes. The red curves that are labeled with the ν' indices in Fig. 1(b) represent the constructive conditions for interference between exposed levels. They are obtained using the interference model, Eq. (5), assuming pinholes that penetrate to the buried interface. They accurately reproduce the *p*-ratio modulations in Fig. 1(b) that are not associated with the x-raylike interference [yellow curves in Figs. 1(a) and 1(b)]. Due to the inverse relation between real space and reciprocal space (the energy scales in Figs. 1 and 2 relates to perpendicular momentum transfer), shallower morphological features, if they would be present, would produce peaks with greater energy separation than are present in Figs. 1(b) and 3. Thus, shallower features must be ruled out. The simplest explanation of morphological features whose heights are always equal to the film thickness during growth is that pinholes are present that penetrate to the interface, thereby exposing bare substrate surface. Although it would be interesting to look at this system again using different experimental techniques, e.g., scanning tunneling microscopy, to confirm pinholes, LEED spot-profile analysis already by itself is a powerful and reliable probe of surface morphology. Therefore, the experimental results that we present should be able to stand on their own as a good indication of the surface morphology.

The oscillation amplitudes in Fig. 3 are used just for making an estimate of the area fraction of the pinholes. We consider the amplitude of intensity oscillations for a 15.3 ML Ag film in Fig. 3, in order to avoid the influence of QW resonance peaks which are stronger for thinner films. Figure 3 also indicates the predicted positions of intensity peaks of different indices, ν', that are produced by pinholes [extracted from Fig. 1(b)] and the expected positions of QW resonance peaks of different indices, ν [also extracted from Fig. 1(a)]. The energy range between 7–14 eV where the *p*-ratio oscillation amplitude is largest in Fig. 3 corresponds to the energy range where the ratio of the reflectivities of bulk Fe(100) and thick Ag(100) films are also the highest (Fig. 2). This argues further for the presence of pinholes that expose the bare Fe substrate surface. It also supports the claim that the reflection from bare Fe at the bottom of pinholes contributes to the oscillation amplitudes.

The formation of pinholes is itself an interesting phenomenon. As noted in the introduction, Ag films should be nearly strain free. Thus, we can rule out a stress-induced effect that gives rise to step undulations and film roughening in other systems.[34–36] The surface energy of Ag(100) is also lower than Fe(100).[37] This rules out thermodynamically driven nonwetting. Alternatively, pinhole formation may result from kinetic limitations. Rough growth of the Ag(111) surface occurs due to a step-edge-diffusion barrier, or Schwoebel-Ehrlich barrier, that hinders motion of atoms down a step.[38–40] On the contrary, smooth growth of Ag(100) at 300 K is a manifestation of the absence of a step-edge barrier.[38,40,41] It is absent on Ag(100) because atoms descend a step by an exchange mechanism, not by hopping.[40] However, an atom that descends a step from the top of the wetting Ag layer in contact with Fe(100) may not do so by exchange. This mechanism could be inhibited by the strong interaction between Ag and Fe which effectively lowers the exposed surface energy and drives wetting in the first place. An atom that must resort to hopping down from on top of the wetting layer may confront a step-edge barrier. This inhibition could easily result in holes in the initial wetting layer. Smooth growth on top of the wetting layer is expected to occur due to the emergence of the exchange mechanism in Ag/Ag(100) growth which suppresses the step-edge barrier. Another kinetic effect that may play a role is the existence of a "three-dimensional (3D) Schwoebel-Ehrlich barrier," which is associated with atomic motion across the corner between macroscopic facets on a crystal.[42–45] The 3D barrier is expected to influence 3D crystal-growth shapes and film texture.[42,43] 3D barriers have been predicted for atomic motion between the (100) plane and other low-index planes for Al, an fcc metal like Ag.[42] Experimental evidence suggests that the 3D barrier affects 3D Ag crystal-growth shapes.[44,45] Together, the presence of a step-edge barrier in the wetting layer, its absence in subsequent Ag layers, and the existence of the 3D barrier may produce pinholes with steep sidewalls.

B. Thermal decomposition

The thermal stability of films grown at room temperature was also investigated by LEEM imaging and $I(V)$ spectra

measurements. These investigations confirmed the stability of 2 and 5 ML films that was reported earlier.[6,10] In agreement with earlier work,[10] we also find that films grown at room temperature with intermediate 3 and 4 ML thickness decompose upon annealing to 2 and 5 ML products that are stabilized by QW states. This behavior is in contrast to an unusual bifurcation mode of thermal decomposition that was observed previously in atomically smooth films prepared at low temperature.[6] We have not examined the decomposition of thicker films in detail. Some difficulty is caused by the weaker quantum-size contrast between different film thickness. Weaker contrast is a consequence of the flatter dispersion of QW resonance conditions [see Fig. 1(a)] at larger thickness.

Different stages of the thermal-decomposition process are revealed in the details of the $I(V)$ spectra that were measured during annealing (Fig. 5). We find that 3 ML films are stable up to about 340 K and thereafter decompose directly into 2- and 5-ML-thick regions upon annealing to higher temperature. The spectra indicate that morphological changes are modest initially in the lower temperature range, 340–372 K, but become much more pronounced at 387 K and above. On the other hand, fairly significant morphological changes in initially 4 ML films are detected in $I(V)$ spectra already at 320 K. The data indicate that this decomposition proceeds initially by bifurcation to 3 and 5 ML thicknesses of at least part of the 4 ML film and continues at 387 K and above with the production of stable 2- and 5-ML-thick regions only. The onset of the latter stages of thermal decomposition of the initial 3 and 4 ML films at coincidentally the same temperature, 387 K, suggests that significant dewetting of the third from the second Ag layer occurs commonly at this temperature in both cases. Therefore, the observation that 4 ML films decompose initially at lower temperature by bifurcation, which involves dewetting of the fourth from the third Ag layer, could argue for a layer-dependent bonding of the topmost to underlying layers. This could itself be QSE induced.

The LEEM observations of morphological changes that occur during the thermal decomposition of unstable 3 and 4 ML films (Fig. 4) reveal the nucleation of many small features that gradually coarsen into distinct 2 and 5 ML regions with large areas. This nucleation behavior is consistent with the presence of numerous, small and randomly located pinholes in the initial films prior to annealing that is also indicated by LEED spot-profile measurements in the present work [Fig. 1(b)]. It was shown previously that the area fractions of the 2 and 5 ML product regions account for all of the material in the initial 3 and 4 ML films.[10] The apparent conservation of mass during decomposition[10] implies that the area fraction of the pinholes must be small. This is corroborated by the small pinhole area fraction that we have estimated roughly here. These observations suggest that pinholes enable a mechanism that promotes the decomposition of the film directly to thicknesses that are stabilized by QW states. The bifurcation mode of thermal decomposition in atomically flat films[6] likewise can be attributed to the combined action of QW state energetics and kinetic limitations that arise in the absence of pinholes.

The origin of this kinetic limitation and an atomistic description of the decay mechanism in the presence of pinholes, however, remain unclear. The decomposition of a flat, defect-free film conceivably begins with the nucleation of an atomic height island on top of the topmost atomic layer of the film and the nucleation of a complementary vacancy island within the same layer. Mass flow between the steps at the edges of the vacancy island and the island is then all that must occur to produce the bifurcation morphologies. In order to produce QW-stated-induce morphologies, additional nucleation of a vacancy island in a deeper layer or of an island at a higher level and mass flow across multiple layers must also occur. The energy barriers that are confronted in these processes are the nucleation barriers associated with forming steps on the edges of islands and vacancy islands and the barriers to mass transport between step edges in different layers (atom detachment, ascending a step, diffusion and reattachment), including the initial adatom-vacancy formation process. The nucleation rates and the rates that atoms are transferred between levels should control the kinetics of decomposition and possibly also the final morphologies. It was pointed out that the energy barrier for island and vacancy island nucleation can be prohibitively high as to prevent morphological changes by this mechanism.[46–48] In this case, a different dewetting mechanism may occur in the presence of substrate steps that avoids two-dimensional island and vacancy island nucleation.[47,48] However, such behavior was not observed here in the case of the thermal decomposition of Ag films grown at room temperature. It probably also did not occur during the thermal decomposition of atomically flat films, which were grown on step-free Fe whiskers.[6] Film dewetting via island and vacancy island nucleation can occur if the driving force is high and the nucleation barrier is low.[49] Such a strong driving force may be provided in the case of Ag/Fe(100) by the QW state energetics. The barriers for nucleating islands at higher levels should be the same for films that are initially atomically flat and for films that are punctuated by pinholes. Therefore, we suspect that the different decomposition modes that have been observed for Ag/Fe(100) films with these different initial morphologies stem from two effects: (1) the absence of a nucleation barrier for vacancy island formation in films with pinholes and (2) the promotion of island nucleation by possibly enhanced mass transport from preexisting steps at the interior edges of these pinholes. The latter of these two effects is believed to be a consequence simply of the number of atomic sites at the perimeter of a pinhole, which is expected to be larger than for a critical vacancy island in an atomically flat film.

IV. CONCLUSION

We find that the predominant morphological defect in Ag films that are grown in a layer-by-layer manner on Fe(100) at room temperature are pinholes that penetrate from film surface to substrate surface. The presence of pinholes in films grown at room temperature and their absence from atomically smooth films grown at low temperature[6] correlates with the different thermal-decomposition modes of these morphologically distinct films. The bifurcation mode of thermal decomposition of atomically smooth films[6] can therefore be

attributed to the combined action of quantum-well state energetics and kinetic limitations associated with nucleation of deeper and higher layers. These kinetic limitations are apparently suppressed in films grown at room temperature by the presence of pinholes. We speculate that pinholes act on the thermal decomposition first of all by eliminating the barrier to vacancy island nucleation. Pinholes may also act to promote island nucleation by serving as a more efficient source for atomic mass transport to higher levels than critical or subcritical vacancy islands. A deeper understanding of the kinetic barriers and processes involved in thermal decomposition and growth of quantum-confining films can lead to greater control over the fabrication of quantum-size-effect-induced nanostructures, which is essential for varying and controlling their electronic structure and properties. Experimental observations were also made that indicate that the bonding of the topmost layer to the underlying film is stronger for a 3 ML film than for a 4 ML film. This effect may itself be QW state induced and thus would be a QSE that has not been identified previously.

ACKNOWLEDGMENT

The authors gratefully acknowledge the Hong Kong Research Grants Council for support under Grant No. HKUST600106.

*Corresponding author; phaltman@ust.hk

[1] F. J. Himpsel, J. E. Ortega, G. J. Mankey, and R. F. Willis, Adv. Phys. **47**, 511 (1998).
[2] T. C. Chiang, Surf. Sci. Rep. **39**, 181 (2000).
[3] M. C. Tringides, M. Jałochowski, and E. Bauer, Phys. Today **60**(4), 50 (2007).
[4] L. Gavioli, K. R. Kimberlin, M. C. Tringides, J. F. Wendelken, and Z. Zhang, Phys. Rev. Lett. **82**, 129 (1999).
[5] K. Budde, E. Abram, V. Yeh, and M. C. Tringides, Phys. Rev. B **61**, R10602 (2000).
[6] D.-A. Luh, T. Miller, J. J. Paggel, M. Y. Chou, and T. C. Chiang, Science **292**, 1131 (2001).
[7] H. Yu, C. S. Jiang, Ph. Ebert, X. D. Wang, J. M. White, Q. Niu, Z. Zhang, and C. K. Shih, Phys. Rev. Lett. **88**, 016102 (2001).
[8] R. Otero, A. L. Vázquez de Parga, and R. Miranda, Phys. Rev. B **66**, 115401 (2002).
[9] L. Floreano, D. Cvetko, F. Bruno, G. Bavdek, A. Cossaro, R. Gotter, A. Verdini, and A. Morgante, Prog. Surf. Sci. **72**, 135 (2003).
[10] K. L. Man, Z. Q. Qiu, and M. S. Altman, Phys. Rev. Lett. **93**, 236104 (2004).
[11] V. Fournée, H. R. Sharma, M. Shimoda, A. P. Tsai, B. Unal, A. R. Ross, T. A. Lograsso, and P. A. Thiel, Phys. Rev. Lett. **95**, 155504 (2005).
[12] B. Unal, F. Qin, Y. Han, D. J. Liu, D. Jing, A. R. Layson, C. J. Jenks, J. W. Evans, and P. A. Thiel, Phys. Rev. B **76**, 195410 (2007).
[13] Y. Han, B. Unal, F. Qin, D. Jing, C. J. Jenks, D. J. Liu, P. A. Thiel, and J. W. Evans, Phys. Rev. Lett. **100**, 116105 (2008).
[14] J. Chen, M. Hupalo, M. Ji, C. Z. Wang, K. M. Ho, and M. C. Tringides, Phys. Rev. B **77**, 233302 (2008).
[15] K. L. Man, M. C. Tringides, M. M. T. Loy, and M. S. Altman, Phys. Rev. Lett. **101**, 226102 (2008).
[16] C. M. Wei and M. Y. Chou, Phys. Rev. B **68**, 125406 (2003).
[17] J. E. Prieto and I. Markov, Phys. Rev. Lett. **98**, 176101 (2007).
[18] M. Henzler, Appl. Phys. A: Mater. Sci. Process. **34**, 205 (1984).
[19] R. Altsinger, H. Busch, M. Horn, and M. Henzler, Surf. Sci. **200**, 235 (1988).
[20] M. Horn-von Hoegen, Z. Kristallogr. **214**, 591 (1999).
[21] W. F. Chung, Y. J. Feng, H. C. Poon, C. T. Chan, S. Y. Tong, and M. S. Altman, Phys. Rev. Lett. **90**, 216105 (2003).
[22] E. Chason and T. M. Meyer, Crit. Rev. Solid State Mater. Sci. **22**, 1 (1997).
[23] M. S. Altman, J. Phys.: Condens. Matter **17**, S1305 (2005).
[24] E. Bauer, Rep. Prog. Phys. **57**, 895 (1994).
[25] M. S. Altman, J. Phys.: Condens. Matter (to be published).
[26] K. L. Man, Y. J. Feng, C. T. Chan, and M. S. Altman, Surf. Sci. **601**, L95 (2007).
[27] G. Fuster, J. M. Tyler, N. E. Brener, J. Callaway, and D. Bagayoko, Phys. Rev. B **42**, 7322 (1990).
[28] N. V. Smith, N. B. Brookes, Y. Chang, and P. D. Johnson, Phys. Rev. B **49**, 332 (1994).
[29] $\Phi_B(E)$ in the QW state/resonance quantization condition is rigorously the internal reflection phase at the surface-potential barrier at energies below the vacuum level, $E<E_{\mathrm{vac}}$. For $E>E_{\mathrm{vac}}$, it is a composite of the external reflection phase in vacuum from the film surface, $\Phi_B'(E)$, and any possible phases that may be introduced upon transmission through the surface with appropriate sign.
[30] J. J. Paggel, T. Miller, and T.-C. Chiang, Phys. Rev. B **61**, 1804 (2000).
[31] A zone-folded scheme was used in Ref. 10 to determine $\kappa(E)$. Here, $\kappa(E)$ is determined from $k(E)$ that is not folded from the second to the first Brillouin zone. Thus, $\kappa(E)$ is negative here while it was positive in Ref. 10, and correspondingly $\Phi_C(E)$ and ν also have opposite sign here compared to Ref. 10.
[32] R. Bertacco and F. Ciccacci, Phys. Rev. B **59**, 4207 (1999).
[33] $\Phi_B'(E)$ should not be confused with $\Phi_B(E)$ in the quantization condition for QW states/resonances, e.g., Eq. (1). $\Phi_B'(E)$ is only the reflection phase in vacuum from the film surface. It is subtracted in the constructive interference condition for spot-profile analysis because we are calculating the phase *difference* between the waves that are reflected from the film and substrate surfaces. See also the comment given as Ref. 29.
[34] C. Roland, MRS Bull. **21**, 27 (1996).
[35] F. Léonard and J. Tersoff, Appl. Phys. Lett. **83**, 72 (2003).
[36] K. L. Man, Q. L. Guo, and M. S. Altman, Surf. Sci. **600**, 1060 (2006).
[37] L. Vitos, A. V. Ruban, K. L. Skiver, and J. Kollár, Surf. Sci. **411**, 186 (1998).
[38] Y. Suzuki, H. Kikuchi, and N. Koshizuka, Jpn. J. Appl. Phys. **27**, L1175 (1988).
[39] H. A. van der Vegt, H. M. van Pinxteren, M. Lohmeier, E. Vlieg, and J. M. C. Thornton, Phys. Rev. Lett. **68**, 3335 (1992).

[40] B. D. Yu and M. Scheffler, Phys. Rev. Lett. **77**, 1095 (1996).
[41] C. R. Stoldt, K. J. Caspersen, M. C. Bartelt, C. J. Jenks, J. W. Evans, and P. A. Thiel, Phys. Rev. Lett. **85**, 800 (2000).
[42] S. J. Liu, H. Huang, and C. H. Woo, Appl. Phys. Lett. **80**, 3295 (2002).
[43] M. G. Lagally and Z. Zhang, Nature (London) **417**, 907 (2002).
[44] W. X. Tang, K. L. Man, H. Huang, C. H. Woo, and M. S. Altman, J. Vac. Sci. Technol. B **20**, 2492 (2002).
[45] K. L. Man, W. X. Tang, H. Huang, and M. S. Altman, in *Kinetics-Driven Nanopatterning on Surfaces*, edited by E. Chason, G. H. Gilmer, H. Huang, and E. Wang (Materials Research Society, Warrendale, 2005), p. 81.
[46] W. W. Mullins and G. S. Rohrer, J. Am. Ceram. Soc. **83**, 214 (2000).
[47] W. L. Ling, T. Giessel, K. Thürmer, R. Q. Hwang, N. C. Bartelt, and K. F. McCarty, Surf. Sci. **570**, L297 (2004).
[48] K. F. McCarty, J. C. Hamilton, Y. Sato, A. Saá, R. Stumpf, J. de la Figuera, K. Thürmer, F. Jones, A. K. Schmid, A. A. Talin, and N. C. Bartelt, New J. Phys. **11**, 043001 (2009).
[49] K. Thürmer and N. C. Bartelt, Phys. Rev. Lett. **100**, 186101 (2008).